JOURNAL OF CATALYSIS 113, 410–433 (1988)

Methanol and C_2 Oxygenate Synthesis over Cesium Doped Cu/ZnO and $Cu/ZnO/Al_2O_3$ Catalysts: A Study of Selectivity and ^{13}C Incorporation Patterns

JOHN G. NUNAN,[1] CHARLES E. BOGDAN,[2] KAMIL KLIER, KEVIN J. SMITH,[3] CHYI-WOEI YOUNG,[4] AND RICHARD G. HERMAN

Department of Chemistry and Zettlemoyer Center for Surface Studies, Lehigh University, Bethlehem, Pennsylvania 18015

Received December 8, 1987; revised April 18, 1988

Cesium formate significantly promotes methanol and C_2 oxygenate (methyl formate MF and ethanol EtOH) synthesis over the Cu/ZnO catalyst. ^{13}C NMR analysis of the product obtained from $^{13}CH_3OH$ and $^{12}CO/H_2$ shows that MF is formed by direct carbonylation of methanol and EtOH is formed by coupling of oxygenated C_1 intermediates originating from methanol. The C_1 coupling mechanism overrides various CO insertion paths to ethanol over the present Cs/Cu/ZnO catalyst. The kinetic significance of C_1 aldehydic species such as adsorbed formyl and formaldehyde is supported by experimental evidence and theoretical calculations.

INTRODUCTION

Promotion of higher alcohol and oxygenate synthesis over methanol synthesis catalysts by doping with alkali metal ions has been shown to occur over both the early reported high-pressure (20.3–25.3 MPa) (1 atm = 0.1013 MPa) and high-temperature (673–723 K) zinc chromite catalysts (*1*) and the newer low-pressure (2–10 MPa) and low-temperature (500–600 K) copper-based catalysts (*2, 3*). One of the earliest studies was conducted by Morgan *et al.* (*4*), where it was shown that the salts of alkali metals, particularly of rubidium and cesium, are effective promoters of higher oxygenate synthesis over a Cr_2O_3/MnO catalyst. Recently, Vedage *et al.* (*5*) reported that over the copper-based catalysts, heavy alkali ions are also effective promoters for higher oxygenate synthesis. However, the effect of alkali doping on the synthesis of methanol has until recently been reported to include mainly the retardation of the reaction and lowering of the selectivity to methanol (*2, 4, 6*). Over transition metal catalysts such as palladium supported on silica (*7*), alkali doping inhibited methanol formation, whereas over copper-based methanol synthesis catalysts, the patent literature (*8*) specifies the absence of alkali from the catalyst composition for the selective synthesis of methanol. However, in 1986 a report from this laboratory demonstrated that heavy alkali, particularly cesium, also promote methanol synthesis when used at optimum surface concentrations (*9*).

Numerous reaction mechanisms have been proposed for methanol synthesis, and the development of mechanistic concepts has been summarized and discussed elsewhere (*10, 11*). The existence of formate and methoxy intermediates on the surface of the Cu/ZnO-based catalysts has been firmly established with the use of techniques such as *in situ* infrared spectroscopy (*12*), chemical trapping (*13, 14*), and isotope labeling (*15*), and more recently the presence of a formyl or aldehydic interme-

[1] Present address: Allied Signal, P.O. Box 5016, Des Plaines, IL 60017.

[2] Present address: J. T. Baker, Inc., 222 Red School Lane, Phillipsburg, NJ 08865.

[3] Present address: Department of Chemical Engineering and Applied Chemistry, University of Toronto, Toronto, Canada M5S 1A4.

[4] Plentiful Industrial Corp., U.S.A., 275 Baldwin St., Suite 201, Parsippany, NJ 07054.

0021-9517/88 $3.00

diate has also been reported (*16–18*). In the case of higher alcohol synthesis, the observation of a formyl or aldehydic intermediate is significant in view of mechanistic proposals put forward as early as that of Morgan *et al.* (*4*), which suggest that the synthesis occurs via the aldol coupling of the C_1 intermediate with other aldehydic intermediates, followed by partial dehydration and hydrogenation. A similar reaction mechanism has recently been invoked by Vedage *et al.* (*5*) and has been used in explaining the promotional effect of alkali metal ions such as cesium in the selective synthesis of higher alcohols, in particular the branched product 2-methyl-1-propanol.

The present paper reports on a mechanistic investigation of the *initial steps of higher oxygenate synthesis* over the Cs/Cu/ZnO catalyst. Aside from methanol, methyl formate and ethanol are the initial side products. The rate of methyl formate formation can be taken as a measure of C–O bond formation and that of ethanol as a measure of C–C bond formation.

The synthesis of *methyl formate* can occur by direct carbonylation of methanol,

$$CH_3OH + CO \rightarrow HCOOCH_3 \quad (1)$$

by dehydrogenative coupling of two methanol molecules,

$$2CH_3OH \rightarrow HCOOCH_3 + 2H_2 \quad (2)$$

or the related Tischenko dimerization of formaldehyde,

$$2HCHO \rightarrow HCOOCH_3 \quad (3)$$

or by the esterification of formic acid with methanol

$$HCOOH + CH_3OH \rightarrow HCOOCH_3 + H_2O \quad (4)$$

The direct carbonylation (1) has been a favored reaction mechanism over alkali alkoxide catalysts (*19–21*) but dehydrogenative coupling of methanol (2), thought to go via methanol dehydrogenation followed by the Tischenko reaction (3), has been suggested for the copper-based catalysts (*22*). A reaction path from formaldehyde and methoxide via a "hemiacetal" intermediate (5) has also been proposed for the copper-based catalysts (*23, 24*) where the reactants are surface-bound species (*25*). The "hemiacetal" intermediate has also been reported (*26*) to be important for the reverse of reaction (5),

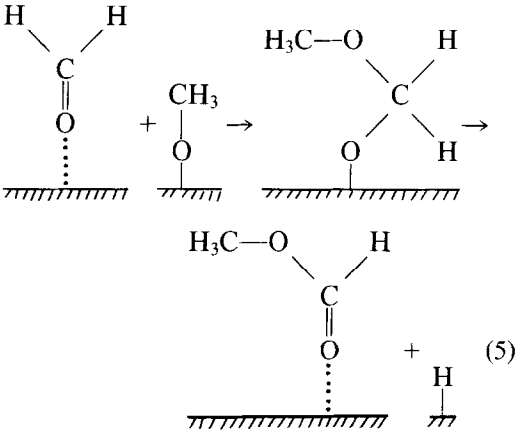

(5)

A hemiacetal mechanism similar to (5) has also been invoked by Vedage *et al.* (*5*) as a general path to methyl esters in higher oxygenate synthesis. However, Smith *et al.* (*27*) found that the rate constant for methyl formate synthesis over the Cs/Cu/ZnO catalysts had a much higher value than that for higher methyl esters, and this result indicates that the mechanism for methyl formate may be different from that for higher esters. Since the Cs/Cu/ZnO catalyst has both the basic alkali component and the hydrogenation–dehydrogenation Cu/ZnO components, it is of interest to determine whether the alkali-catalyzed carbonylation reaction (1) prevails on this catalyst over reactions (2)–(4) that require dehydrogenation of methanol.

The synthesis of *ethanol* has also been proposed to occur by several paths. These can be divided into three principal categories: direct synthesis from CO/H_2,

$$2CO + 4H_2 \rightarrow C_2H_5OH + H_2O \quad (6)$$

homologation of methanol by CO/H_2,

$$CH_3OH + CO + 2H_2 \rightarrow C_2H_5OH + H_2O \quad (7)$$

and coupling of two methanol molecules

$$2CH_3OH \rightarrow C_2H_5OH + H_2O \quad (8)$$

Reaction (6) has been proposed for the synthesis of ethanol over supported Rh catalysts (*28, 29*), while reaction (7) has been employed to describe alcohol formation in Fischer–Tropsch synthesis (*30–33*) and in higher alcohol synthesis over alkali/Cu-based (*1, 5, 34*) or other (*35*) catalysts. The synthesis of ethanol over unspecified high-pressure alcohol synthesis catalysts has been proposed by Graves (*36*) to occur by reaction (8), and higher alcohols would be formed by analogous coupling reactions. A modification of reaction (8) has been invoked for alcohol synthesis over alkali acetylide catalysts (*37*) in which C_1 aldehydic intermediates are the reactants,

$$2CH_3OH \xrightarrow{-2H_2} 2H_2CO \rightarrow CH_2OH \cdot CHO \xrightarrow[-H_2O]{2H_2} C_2H_5OH. \quad (9)$$

The various classes of methyl formate and ethanol-forming mechanisms can be distinguished by experiments in which the source of carbon atoms of the C_2 oxygenates is traced to carbon monoxide or to methanol. The reactions of isotopically labeled mixtures of $^{13}CH_3OH$ and $^{12}CO/H_2$ were used to this end, and the appearance of ^{13}C in each individual carbon of methyl formate and ethanol (and propanol) has been followed and quantitatively analyzed by ^{13}C NMR of the collected product. The results of the analysis presented below show that the dominant source of the methyl (carbonyl) group of the methyl formate is methanol (carbon monoxide) and the dominant source of both carbons of ethanol is methanol. This synthesis pattern is consistent with the dominance of path (1) for methyl formate and of path (8) or (9) for ethanol. Independent evidence from previous studies indicate the kinetic significance of surface aldehydic intermediates (*15, 18*) and favors the aldehyde coupling reaction (9) over the alcohol coupling reaction (8) for ethanol synthesis over the present Cs/Cu/ZnO catalyst.

EXPERIMENTAL

Catalyst preparation involved the initial precipitation of the hydroxycarbonate precursor, identified as aurichalcite ($Cu_{1.5}Zn_{3.5}(CO_3)_2(OH)_6$) by Himelfarb *et al.* (*38*), by previously described procedures (*39*) followed by stepwise calcination to 623 K to give the CuO/ZnO = 30/70 mixture. Cesium doping with CsOOCH in aqueous solution was carried out either after precursor calcination, the catalyst so prepared being termed "calcined-doped," or after reduction of the catalyst in 2% H_2/N_2 at 523 K, termed "reduced-doped" catalyst. In the latter case, the catalysts were prepared by removing the reduced catalyst (Cu/ZnO) from the reactor under N_2 and adding 2.5 g to 25 ml of N_2-purged CsOOCH solution at 323 K. The solution was then evaporated to dryness under flowing N_2, and the resulting doped catalyst was reintroduced into the reactor under N_2 for the determination of its activity. Both doping procedures have been shown to deposit the alkali salt in a molecularly dispersed submonolayer. Quantitative X-ray photoelectron spectroscopic (XPS) analysis led to the conclusion that the alkali salt was located predominantly on the zinc oxide component of the catalyst (*40*).

A ternary Cu/Zn/Al catalyst was also prepared by initial precipitation of a hydroxycarbonate precursor (*41–43*), which in this case had a hydrotalcite structure (*44*). Hydrotalcite is a naturally occurring mineral having the typical composition of $Mg_6Al_2(OH)_{16}CO_3 \cdot 4H_2O$, whereas the catalyst precursor prepared here contained Cu and Zn in place of the magnesium and was isomorphous with the natural mineral. The hydrotalcite-like precursor was subsequently calcined at 623 K in the usual manner to give the oxide form of the catalyst

and then doped with cesium as previously described for the calcined-doped binary CuO/ZnO catalyst. Before being subjected to the reaction conditions, the catalyst was reduced in 2% H_2/N_2 at ambient pressure at 523 K. The reduction process was monitored by gas chromatographic analysis of water in the exit gas and was terminated when a sudden decrease in the production of water was observed. Such a reduction resulted in a catalyst that was black (*45*) and had a high activity (*39*).

Catalyst testing was carried out in a fixed bed continuous flow reactor operating at a total pressure of 7.6 MPa. Details of reactor construction and mode of operation have been described previously (*39, 46*). Portions of 2.45 g of the Cs/Cu/Zn catalyst having a particle diameter between 0.85 and 2.0 mm were used, and the catalyst was diluted with approximately three times its volume with 3-mm Pyrex beads. The exit gas from the reactor was sampled every 22–60 min using an in-line automated heated sampling valve and analyzed in a Hewlett–Packard 5730A gas chromatograph that was coupled with a Model 3388A integrator–controller unit. Reaction products were separated on a Poropak Q column and were identified by comparison of their retention times with those of known standards and also from their mass spectroscopic fragmentation patterns, as determined with the use of a Finnegan-4000 GC/MS spectrometer.

Initial catalyst activities were determined at 523 K with a synthesis gas composition of $H_2/CO = 2.33$, gas hourly space velocity (GHSV) = 6120 liters (STP)/kg cat./h, and at a total pressure of 7.6 MPa. The steady-state activities established after 24 h under these conditions were used to compare the methanol synthesis rates over the different cesium doped catalysts. Under these reaction conditions, methyl formate, ethanol, carbon dioxide, and traces of methane and water were the only side products. Under more severe reaction conditions of higher temperatures and lower GHSV with a $H_2/CO = 4.5$ synthesis gas, 1-propanol, methyl acetate, and 2-methyl-1-propanol were also detected and analyzed.

The mechanism of the formation of lower oxygenates such as methyl formate, ethanol, and 1-propanol over a 0.4 mol% Cs/Cu/ZnO catalyst was studied by the use of ^{13}C-enriched methanol that was injected continuously into the synthesis gas flowing over the catalyst operating under steady-state synthesis conditions. The methanol was enriched by a factor of 22.3 over the natural carbon-13 abundance of 1.11 at.%. The enriched methanol was introduced into the synthesis gas feed at the inlet of the reactor using a high-pressure Gilson Model 302 pump. The injection rate was such that the carbon introduced as methanol did not exceed 10% of the total carbon introduced as carbon monoxide and the concentration of injected methanol was *substantially* less than the equilibrium methanol concentration for the reaction conditions used, T = 490–543 K, P = 7.6 MPa, and H_2/CO = 0.45. Under these conditions, methanol decomposition, and thus scrambling of the ^{13}C label between methanol and the reactant carbon monoxide, was suppressed and the system was not significantly perturbed by the injected methanol. During the ^{13}C-enriched methanol injection experiments, and also control experiments using methanol containing natural abundance ^{13}C carried out under identical conditions, the reaction products were collected using liquid nitrogen traps placed downstream from the back pressure regulator and transferred to NMR tubes that were subsequently sealed. The ^{13}C spectra were obtained with a JEOL FX90Q Fourier transform NMR spectrometer using broadband proton decoupling. Quantitative measurements were made by suppressing the nuclear Overhauser effect using a gated decoupling sequence and utilizing a 45° pulse angle with sufficiently long pulse delays (10 s). Quantitative analysis of ^{13}C in each carbon was made by peak height measurements based on calibrations of ^{13}C signals from mixtures of alcohols of known composition.

Surface areas of the tested and untested

catalysts were determined by the BET method using argon gas, assuming an area of 0.168 nm^2/argon atom (*47*). Samples were loaded under N_2 into the BET apparatus, evacuated overnight, and subsequently heated under vacuum for 1 h at 383 K prior to the surface area measurement at 77 K.

RESULTS

Before the effect of cesium doping on the rate of methanol and higher oxygenate synthesis was studied in detail, conditions were established such that reaction rates were obtained when the reactor was operating in the differential mode. A detailed analysis (*48*) further showed that external mass and heat transfer, plus intraparticle diffusion limitations, were negligible in the case of the Cu/ZnO catalyst under the reaction conditions employed in this investigation. The activities and apparent activation energies of various cesium doped binary catalysts were subsequently obtained under these conditions.

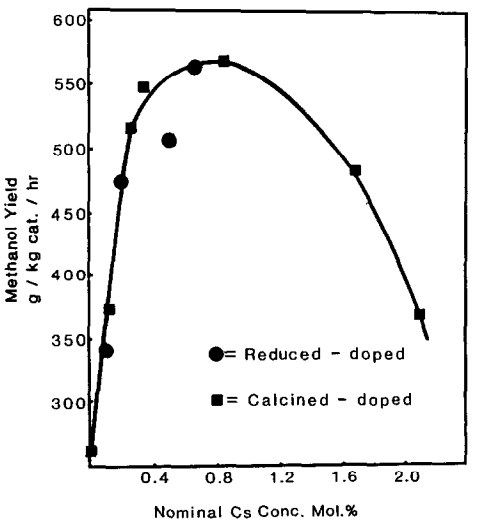

FIG. 1. Yield of methanol as a function of cesium loading over the calcined-doped (■) and reduced-doped (●) binary Cu/ZnO catalyst. Testing conditions: T = 523 K, P = 7.6 MPa, H_2/CO = 2.33, catalyst weight = 2.45 g, GHSV = 6120 liters (STP)/kg cat./h.

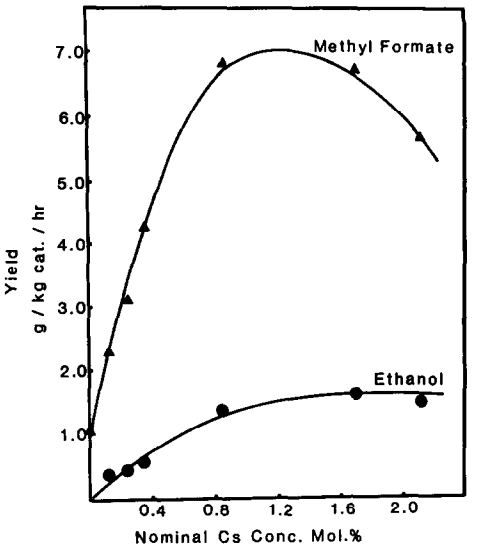

FIG. 2. Yield of methyl formate (▲) and ethanol (●) as a function of cesium loading over the calcined-doped Cu/ZnO catalyst. Experimental conditions are given in Fig. 1.

Effect of Cesium Content on Activity and Selectivity

In Fig. 1 is shown the effect of cesium loading on the rate of methanol formation over the binary Cu/ZnO catalyst at 523 K, 7.6 MPa, and H_2/CO = 2.33. It is evident that the two different preparations, reduced-doped and calcined-doped catalysts, produced identically active catalysts. Up to 0.4 mol% loading of cesium, the activity for methanol formation increased rapidly from 260 to 550 g/kg cat./h, beyond which the rate passed through a broad maximum at 0.8 mol% cesium followed by a decrease in activity. The effects of cesium loading on the methyl formate and ethanol formation over the calcined-doped Cu/ZnO catalysts are shown in Fig. 2. The surface cesium dopant promoted the formation of both products, with methyl formate, like methanol, passing through a distinct maximum but at a higher cesium concentration of 1.2 mol%. The activity for ethanol increased from zero at a 0.0 mol% cesium doping level to reach a plateau at cesium concentrations greater than 1.5 mol%. However,

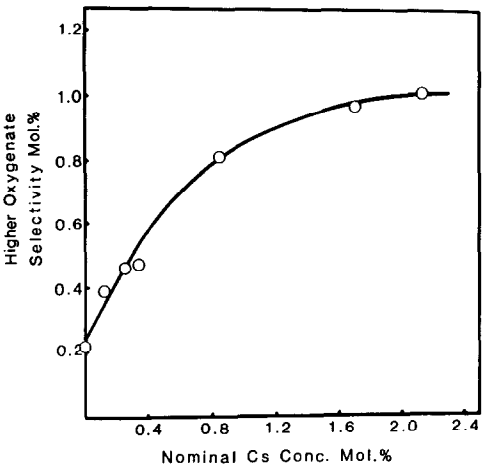

FIG. 3. Plot of selectivity for higher oxygenate formation (defined as mol% of methyl formate + ethanol in the product mixture) as a function of cesium loading over the calcined-doped Cu/ZnO catalyst. Experimental conditions are given in Fig. 1.

even at the highest cesium concentration of 2.13 mol%, ethanol and methyl formate accounted for less than 1.1 mol% of the product, as demonstrated in Fig. 3.

Surface areas of the calcined-doped catalysts were determined before and after catalyst testing. Doping with higher levels of cesium led to a moderate drop in surface area as shown in Fig. 4. Testing also led to a

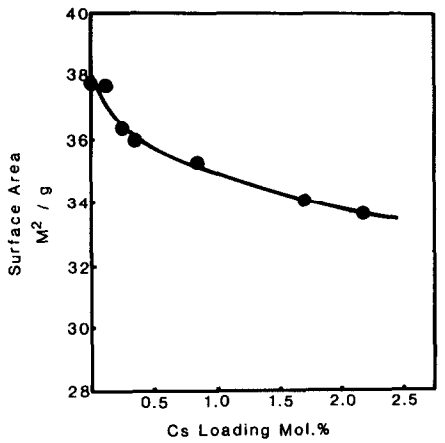

FIG. 4. Surface areas of the tested cesium calcined-doped catalysts (after 24 h of testing) as a function of cesium loading. Experimental conditions are given in Fig. 1.

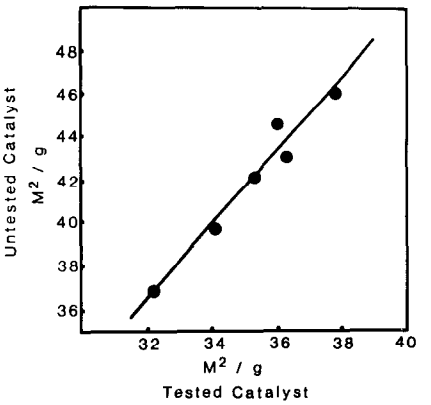

FIG. 5. Relationship between the surface areas of the cesium calcined-doped catalysts before and after testing (Note that surface areas before testing were measured after doping and before reduction.) Experimental conditions are given in Fig. 1.

drop in surface area for all the samples as represented in Fig. 5. A similar result was found for the reduced-doped catalysts. Using the measured surface areas of the tested calcined-doped catalysts, the activities in Fig. 1 were replotted in the form of activity per unit surface area of the catalyst vs the cesium coverage expressed as cesium ions per square meter of catalyst and the resulting plot is presented in Fig. 6. XPS analyses of the tested catalysts showed that within experimental error the cesium was highly dispersed in submonolayer form on the catalyst surface, primarily over the ZnO phase, with no clustering occurring. The initial analyses and data treatments have been reported (*5, 40, 49*). Maximum activity for methanol occurred when the Cu/ZnO catalyst was doped with 15.0×19^{17} cesium ions/m^2 of the total (Cu + ZnO) surface area, which corresponds to a fractional surface area coverage, θ_{Cs}, equal to 0.17. For methyl formate and ethanol, maximum activity occurred at $\theta_{Cs} = 0.26$ and >0.32, respectively.

Effect of Temperature on Oxygenate Synthesis

The effect of reaction temperature on the reaction rate and selectivity was studied in

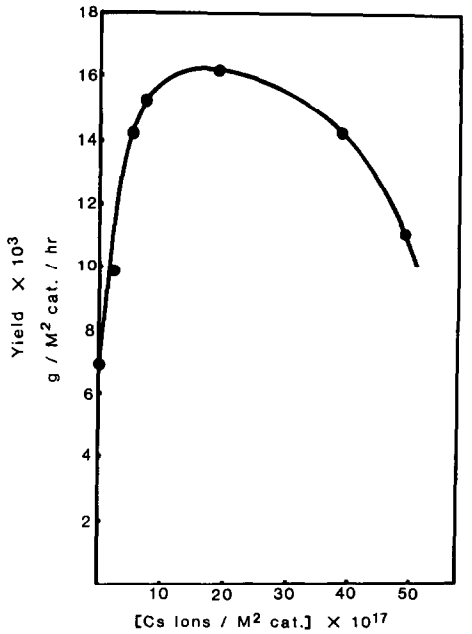

FIG. 6. Methanol yield (specific activity) as a function of cesium loading over the calcined-doped Cu/ZnO catalyst. Experimental conditions are given in Fig. 1.

detail over the 0.34 mol% cesium calcined-doped catalyst, $\theta_{Cs} = 0.17$. Up to 523 K, linear Arrhenius plots were obtained for the rate of formation of both methanol and methyl formate, with ethanol not being detected in the product composition except in trace quantities at the higher temperatures. At the higher temperatures the rates of the formation of ethanol and of ethanol plus higher oxygenates (methyl acetate + 1-propanol) gave linear Arrhenius plots as shown in Fig. 7. Methyl acetate and 1-propanol accounted for 4 to 14 mol% of the C_2^+ oxygenate composition. The apparent activation energies calculated from the Arrhenius plots are summarized in Table 1.

The effect of reaction temperature on the yield of methanol and higher oxygenates was also studied over a 0.8 mol% cesium doped Cu/Zn/Al catalyst, the results of which are summarized in Figs. 8 and 9. In this case, the ratio of H_2/CO employed was 0.45 so as to promote higher oxygenate synthesis. In Fig. 9 are represented the effects

TABLE 1

Comparison of the Apparent Activation Energies for Methyl Formate, Methanol, and Ethanol Formation over the 0.34 mol% Calcined-Doped Cu/ZnO Catalyst from $H_2/CO = 2.33$ Synthesis Gas at 7.6 MPa and with GHSV = 6120 liters (STP)/kg cat./h

Product	E_A^{App} (kJ mol^{-1})	Temperature range (K)
Methyl formate	79.6[a]	488–523
Methanol	73.9[b]	483–523
Ethanol	148.5[c]	532–563

[a] Estimated from the following data points (T (K), rate (mol − (kg cat.)$^{-1}$ hr^{-1})): (488, 0.0218); (493, 0.0296); (523, 0.0871).

[b] Estimated from the following data points (T (K), rate (mol − (kg cat.)$^{-1}$ hr^{-1})): (483, 3.511); (488, 4.709); (493, 5.685); (523, 15.41).

[c] From Arrhenius plot for ethanol in Fig. 7.

of temperature on the rates of methyl formate and ethanol plus higher oxygenates. As expected, the selectivity for higher oxygenates increased rapidly with temperature, the Arrhenius plot slope for higher oxygenate synthesis being greater than that

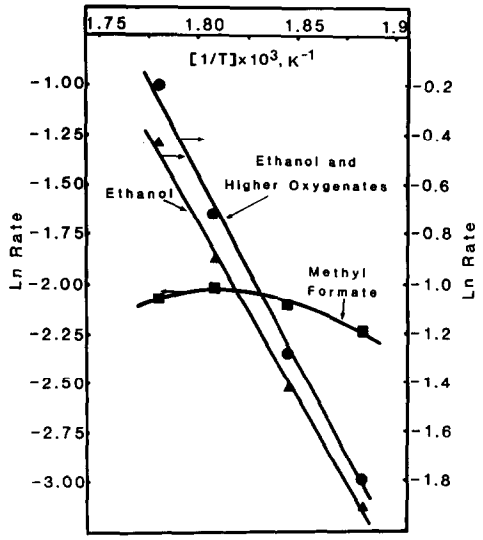

FIG. 7. Arrhenius plots for methyl formate (■), ethanol (▲), and ethanol + higher oxygenate (●) formation over the 0.34 mol% cesium calcined-doped catalyst. Experimental conditions are given in Fig. 1.

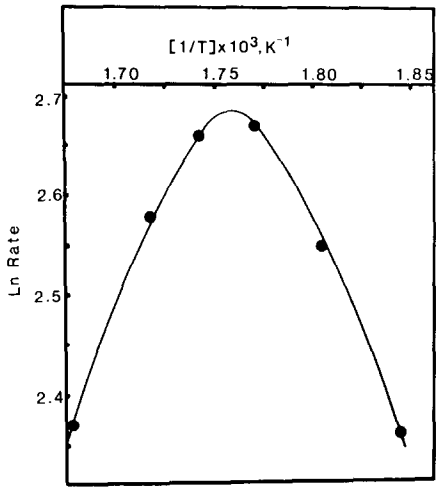

FIG. 8. Arrhenius plot for methanol formation over the ternary 0.8 mol% cesium calcined-doped Cu/Zn/Al catalyst. P = 7.6 MPa, H_2/CO = 0.45, catalyst weight = 2.45 g, GHSV = 3260 liters(STP)/kg cat./h.

for ethanol that tended to level off at higher reaction temperatures.

Injection of Native and ^{13}C-Enriched Methanol

The effect of injecting methanol and ^{13}C-enriched methanol into the synthesis gas feed under steady-state conditions was determined by on-line GC analysis of the gaseous product and ^{13}C NMR analysis of the collected liquid product samples. Spectra of the liquid product collected during injections of the native and ^{13}C-enriched methanol are shown in Figs. 10 and 11 for the synthesis temperatures of 490 and 513 K. The product molar fractions determined by gas chromatography were identical for both the native and the isotopically enriched methanol injected at each reaction temperature. At 490 K, methanol, methyl formate, and traces of water and carbon dioxide were the only products formed. Methanol gave rise to a single ^{13}C NMR peak centered at 49.0 ppm, whereas methyl formate gave rise to a carbonyl carbon peak at 162.2 ppm and a methyl carbon peak at 50.2 ppm. In the experiments with the native [^{13}C]methanol injection, the peak heights of the carbonyl and methyl groups of the methyl formate product were identical, and the molar fractions of methyl formate and methanol as determined from the NMR peak heights agreed well with those obtained from GC product analysis. The results shown in Table 2 demonstrate the quantitative aspects of the ^{13}C NMR analysis.

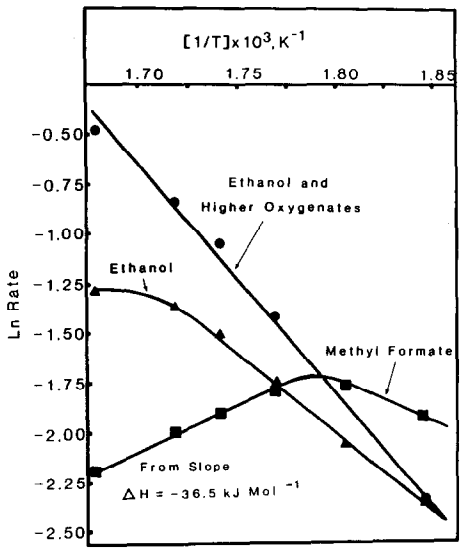

FIG. 9. Arrhenius plots for methyl formate (■), ethanol (▲), and ethanol + higher oxygenates (●) over the ternary 0.84 mol% cesium, calcined-doped Cu/Zn/Al catalysts. Experimental conditions are given in Fig. 8.

For the ^{13}C-enriched methanol injection experiments, comparison of the relative peak heights of the methyl and carbonyl groups of methyl formate clearly showed substantial enrichment of the methyl group relative to the carbonyl carbon. This indicated that CO from the synthesis gas was reacting with the injected methanol as illustrated in

$$*CH_3OH + CO \rightarrow HC(=O)-O*CH_3 \quad (1)$$

It was further observed that the signals of the carbonyl carbon for both the blank and the ^{13}C-enriched experiments were nearly equal (both spectra were obtained under identical instrumental operating conditions), thus providing evidence that the car-

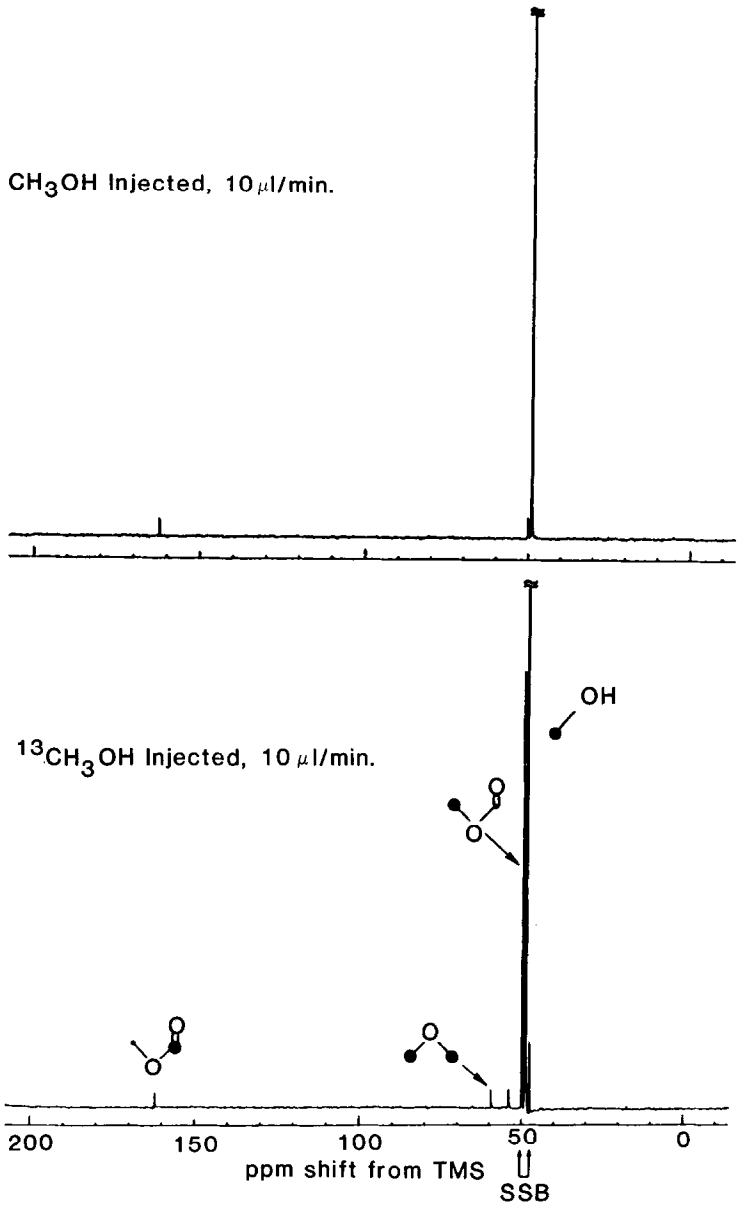

FIG. 10. Effect of injecting methanol and ^{13}C-enriched methanol into the synthesis gas feed under steady-state conditions at 490 K on the ^{13}C NMR spectra of the liquid product. Catalyst is 0.4 mol% Cs/Cu/ZnO, catalyst weight = 2.45 g, methanol injection rate = 194 g/kg cat./h, ^{13}C enrichment = 22.3, GHSV (CO + H_2) = 3260 liters(STP)/kg cat./h, H_2/CO = 0.45, P = 7.6 MPa. The peak at 54 ppm is probably due to the methyl group of a hemiacetal.

bonyl carbon in methyl formate originated from CO and not from the injected [^{13}C]methanol. An identical result was obtained at 513 K; i.e., the methyl carbon in methyl formate was substantially enriched relative to the carbonyl carbon while little or no enrichment was observed in the carbonyl carbon. At 513 K, ethanol was also observed in the product by GC and NMR. The ^{13}C NMR resonance of the C-1 carbon

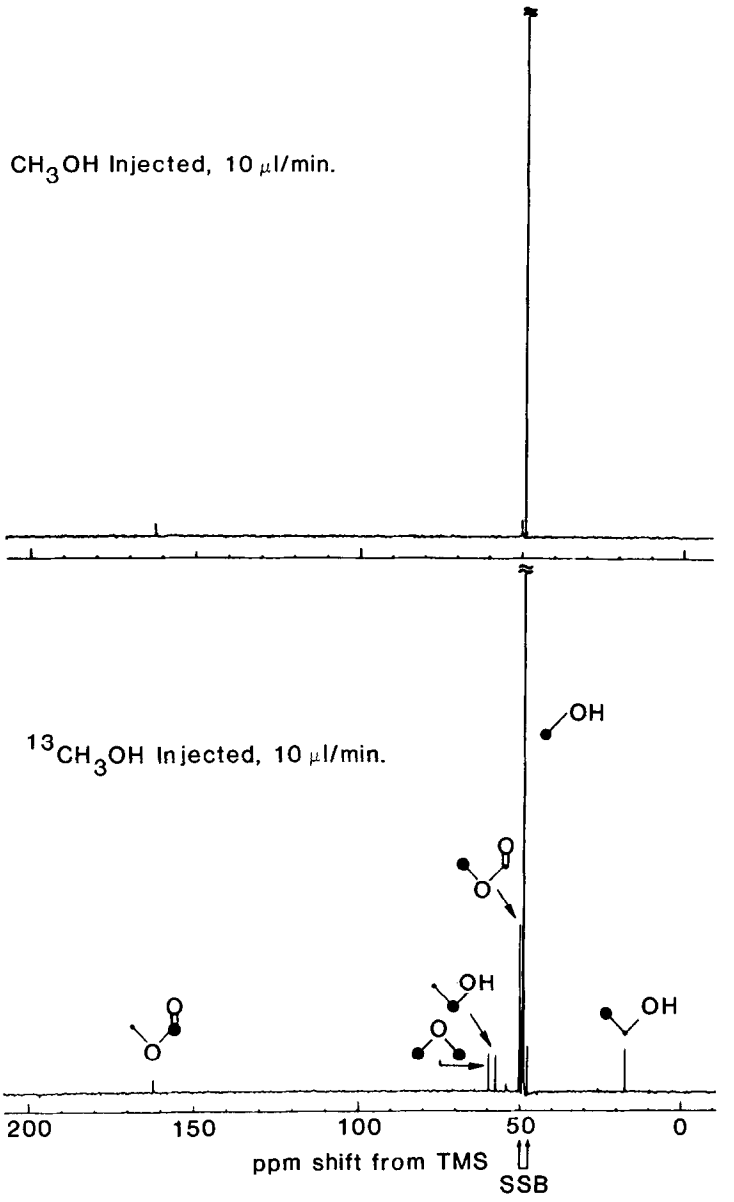

FIG. 11. Effect of injecting methanol and ^{13}C-enriched methanol (24.7% $^{13}CH_3OH$) into the synthesis gas feed under steady-state conditions at 513 K on the ^{13}C NMR spectra of the liquid product. Other experimental conditions are given in Fig. 10.

of ethanol was centered at 57.4 ppm and the C-2 carbon at 17.6 ppm. Comparison of the peak heights for the native ^{13}C and ^{13}C-enriched methanol injection experiments clearly showed that (i) enrichment of both carbons of ethanol had occurred and (ii) both carbons were enriched to the same extent. This isotope distribution is a result of the $C_1 \rightarrow C_2$ synthesis mechanism and not of isotopic scrambling in ethanol as evidenced by the retention of the ^{13}C label in $^{12}CH_3{}^{13}CH_2OH$ injected under identical synthesis conditions (*50*).

In an attempt to exploit the ^{13}C NMR ex-

TABLE 2

Comparison of the Quantitative Analysis of the Collected Liquid Products Produced over the 0.4 mol% Cs/Cu/ZnO Catalyst during Nonenriched Methanol Pumping Experiments

Temperature (K)	Compound analyzed	mol% Composition of product	
		By GC	By NMR
490	Methanol	96.81	97.50
	Methyl formate	3.19	2.50
513	Methanol	97.34	98.06
	Methyl formate	2.44	1.94
	Ethanol	0.22	0.00
553	Methanol	95.80	94.93
	Methyl formate	1.50	1.55
	Ethanol	2.05	2.59
	1-Propanol	0.65	0.93

Note. Reaction conditions are given in Fig. 10.

periments to the fullest, a detailed analysis was carried out for the injection experiments over the temperature range 490–543 K. The product molar fractions determined by GC were used to calculate the enrichments of each carbon center observed by NMR. Using the results from experiments using nonenriched methanol, it was found that the carbon mol fraction ratio (C_x) as determined by GC and NMR (C_x^{NMR}/C_x^{GC}) for each of the products varied from 0.9 to 1.1 (1.0 ± 0.1) for the major products and from 0.7 to 1.3 (1.0 ± 0.3) for the minor products. The greater error observed for the higher oxygenates was due to their very low concentrations in the product mixture, typically less than 5.0 mol%. The low conversions used were selected for the isotope studies since methyl formate, for example, equilibrated with methanol when present in concentrations of 1 to 2 mol%. Therefore, the reaction conditions were chosen such that the yield of methyl formate was far from equilibrium, hence allowing information to be obtained only for the forward reaction.

Taking into account the observation that the carbonyl group of methyl formate was not enriched by ^{13}C during the [^{13}C]methanol injection experiments, the carbonyl carbon could be used as an internal standard. The degree of enrichment of the oxygenate product could be calculated by combining the GC chemical analysis and the observed NMR spectra. Setting the degree of enrichment of the carbonyl carbon equal to 1, relative enrichment factors were calculated for each carbon center of the products collected during the ^{13}C-enriched methanol injection experiments. The results are summarized in Table 3 (also see Fig. 12) and the corresponding GC analytical data are given in Table 4. From the data presented in Table 3 it is evident that the methanol in the product oxygenate mixture had retained the ^{13}C label. Some decomposition of methanol to CO and H_2 occurred as indicated by the ^{13}C balance calculations

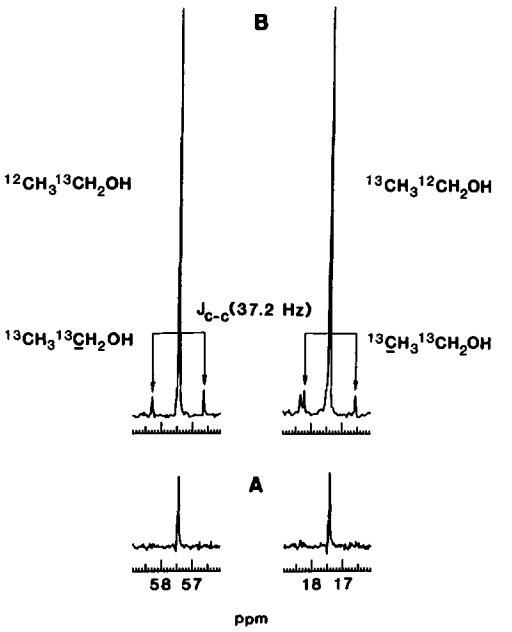

FIG. 12. Comparison of the ^{13}C NMR spectra in the parts per million range encompassing the main peaks of ethanol and the doublets arising from ^{13}C–^{13}C coupling for nonenriched (A) and ^{13}C-enriched (B) methanol injection experiments at 543 K. Other experimental conditions are given in Fig. 10. The peak at 18.3 ppm is identified as the ^{13}C resonance of the methyl groups of 2-methyl-1-propanol.

TABLE 3

Carbon Labeling of the Products Formed During Injection of Enriched [^{13}C]Methanol into the Synthesis Gas as a Function of Reaction Temperature

Product	Enrichment factor for individual carbons					
	490 K	501 K	513 K	523 K	532 K	543 K
CH_3OH	18.9	17.4	10.9	11.9	8.0	7.0
CH_3 | O | C=O H	22.1 1.0	11.2 1.0	10.7 1.0	12.3 1.0	5.7 1.0	5.8 1.0
CH_3[a] | CH_2OH	— —	— —	13.6[b] 11.0[b]	20.2(10.7) 17.7(9.7)	7.5(12.3) 6.0(12.1)	9.0(10.9) 7.9(11.0)
CH_3 | CH_2 | CH_2OH	— — —	— — —	— — —	— — —	9.7[b] 6.5[b] 5.4[b]	4.8[b] 6.4[b] 7.4[b]

[a] The numbers in parentheses are percentages of the ^{13}C atom of the given carbon that are exchange-coupled with nearest neighbor ^{13}C as determined from the observed satellite-to-main resonance ratios as in Fig. 12.

[b] No satellite peaks due to ^{13}C–^{13}C exchange coupling could be determined due to the low concentration of the product molecule and low signal-to-noise ratio.

summarized in Appendix I. It is evident, however, that the 0.02 to 0.70% enrichment of CO by ^{13}C form $^{13}CH_3OH$ decomposition cannot account for the enrichment of the carbons of the products if CO were the carbon source for their synthesis. Further, based on the carbon balances between the reactants and the products (better than 0.2%), ^{13}C could not be lost to unaccounted for compounds such as carbon or waxes deposited on the catalyst surface. Upon increasing the reaction temperature, the enrichment factor for the methanol carbon decreased from 18.9 at 490 K to 8.0 at 543

TABLE 4

Quantitative Analysis of the Same Liquid Products as Those Used for Table 3 as Collected over the 0.4 mol% Cs/Cu/ZnO Catalyst during ^{13}C-Enriched Methanol Injection Experiments

Product	mol% Composition of the product					
	490 K	501 K	513 K	523 K	532 K	543 K
Methanol	96.29	96.91	97.07	97.13	97.36	96.83
Methyl formate	3.71	3.09	2.71	2.41	1.97	1.78
Ethanol	—	—	0.22	0.39	0.55	1.08
1-Propanol	—	—	—	0.07	0.12	0.31

K. This is accounted for partly by dilution of the label with native methanol synthesized over the catalyst and partly by increased extent of methanol decomposition at the higher temperatures. Even at the highest temperatures employed (543 K), the total injected and synthesized methanol ($CH_3OH/CO/H_2 \cong 0.089/0.667/0.244$) was still at significantly less than equilibrium concentration ($CH_3OH/CO/H_2 = 0.232/0.764/0.004$). A detailed analysis of the ^{13}C distribution in ethanol is presented in the discussion for the purpose of distinguishing the various classes of C–C bond-forming reaction mechanisms.

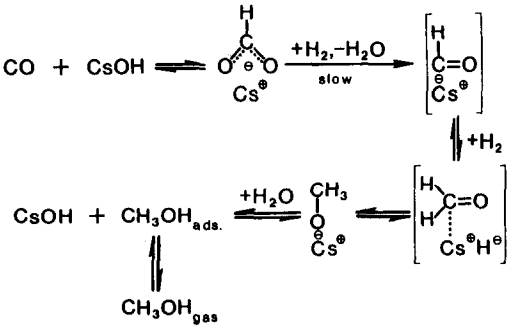

SCHEME I. Methanol synthesis.

DISCUSSION

Methanol Synthesis

The synthesis results presented in Figs. 1, 2, and 3 demonstrate that doping the binary catalyst with cesium gives rise to a substantial promotion of methanol and higher oxygenate synthesis. Figure 3 further shows that promotion of methanol synthesis by a factor of 2.2 or greater can be achieved at low temperatures and high H_2/CO ratios while maintaining the high selectivity for methanol at 98.9 mol%. The observed promotion by cesium was further shown in Fig. 6 to be related to an increase in the *specific* activity of the catalyst surface and not to increases in surface area upon doping (Figs. 4 and 5). Both the number and the reactivity of the active sites on the catalyst surface are increased by cesium doping.

The essential features of methanol synthesis have been discussed previously for the unpromoted binary Cu/ZnO catalyst (*15*). With the present Cs promoted catalyst, the role of Cs^+ in CO activation via association with its ^-OH counterions, shown in Scheme I, is supported by recent *in situ* IR studies (*51*) that have shown that contacting Cs/ZnO or Cs/Cu/ZnO (0.4/5.0/94.6) with $CO + H_2$ led to the formation of a unique CsOOCH species on the catalyst surface. Further hydrogenation of the Cs formate is thought to be the rate-limiting step for the synthesis of methanol by the pathway represented by Scheme I. The slow hydrogenation of formate has also been observed for surface formates on ThO_2 (*52*) and the formate has been proposed as a reaction intermediate in methanol synthesis over these catalysts (*15, 52*). On the other hand, gaseous methanol has been shown to readily react with basic metal oxides such as ZnO to form initially a physisorbed species (*53*) that rapidly forms adsorbed methoxide, a species also formed from synthesis gas-derived formyl (*54*).

In Scheme I, intermediates associated with Cs^+ in square brackets are unproven and their existence is only inferred from their reaction patterns with higher alcohols, aldehydes, ketones, and amines. In particular, the hydride may not be associated with cesium but rather (i) with centers induced by copper species as indicated in thin film model studies (*55*) or (ii) as a CuH moiety that is thought to be significant in copper catalyzed homogeneous methanol synthesis (*56*).

An important result of the present study is the observation of distinct maxima in both methanol and higher oxygenate synthesis rates as a function of cesium loading. Thus, the effect of cesium loading on the rate is reminiscent of previous results on the effects of CO_2 (*57*) and H_2O (*15*), where it was observed that small levels of both

gases promoted methanol synthesis, followed by retardation at higher concentrations. As in the case of water promotion (*15*), the existence of a maximum in methanol synthesis as a function of cesium loading can be explained by the bifunctional nature of the catalyst, whereby the introduction of cesium increases the number of CO activating sites. At higher coverages of cesium the hydrogenation function of the catalyst is suppressed, and this leads to the lowering of activity. The coverage of cesium necessary for maximum activity increases from methanol to methyl formate to ethanol, indicating, as might be expected, that the synthesis of esters and higher alcohols requires even more CO activation than the synthesis of methanol. The synthesis maximum of ethanol does not coincide with that of methanol (Figs. 1 and 2) and can be explained as follows: (i) ethanol synthesis is less sensitive to Cs poisoning of hydrogenation sites and (ii) Cs has the added effect of making the C_1 aldehydic intermediate more reactive in the $C_1 \rightarrow C_2$ step. This is also consistent with previous results that showed that higher alcohol synthesis was favored at lower H_2/CO ratios (*1, 2, 5, 58*). The synthesis pathways that yield methyl formate and ethanol are discussed in the sections that follow.

Formation of Methyl Formate

Several mechanistic and thermodynamic features were considered to account for the observed upper limit of methyl formate formation shown in Fig. 7. These included the questions of whether methyl formate had reached thermodynamic equilibrium at $T >$ 530 K under the present reaction conditions for a reaction stoichiometry indicated in (1)–(4) below and whether methyl formate was a reaction intermediate leading to ethanol or higher oxygenates. In order to determine whether the methyl formate yield was thermodynamically controlled, several reaction equilibria leading to its formation were considered, and the theoretical K_{eq} values were calculated (*59*) as

Direct carbonylation of methanol with CO

$$CH_3OH + CO \rightarrow CH_3{-}O{-}\overset{\overset{O}{\|}}{C}{-}H \qquad (1)$$
$$\Delta G^\circ_{523} = +33.4 \text{ kJ mol}^{-1}$$
$$\Delta H^\circ_{523} = -37.77 \text{ kJ mol}^{-1}$$
$$K_{eq_{523}} = 4.614 \times 10^{-4}$$

Dehydrogenation of methanol

$$2CH_3OH \rightarrow CH_3{-}O{-}\overset{\overset{O}{\|}}{C}{-}H + 2H_2 \qquad (2)$$
$$\Delta G^\circ_{523} = +6.62 \text{ kJ mol}^{-1}$$
$$\Delta H^\circ_{523} = +60.56 \text{ kJ mol}^{-1}$$
$$K_{eq_{523}} = 2.18 \times 10^{-1}$$

Formaldehyde dimerization (Tischenko reaction)

$$HCHO + HCHO \rightarrow CH_3{-}O{-}\overset{\overset{O}{\|}}{C}{-}H \qquad (3)$$
$$\Delta G^\circ_{523} = -46.77 \text{ kJ mol}^{-1}$$
$$\Delta H^\circ_{523} = -116.44 \text{ kJ mol}^{-1}$$
$$K_{eq_{523}} = 4.69 \times 10^{4}$$

Esterification of formic acid with methanol

$$HCOOH + CH_3OH \rightarrow CH_3{-}O{-}\overset{\overset{O}{\|}}{C}{-}H + H_2O \qquad (4)$$
$$\Delta G^\circ_{523} = -13.39 \text{ kJ mol}^{-1}$$
$$\Delta H^\circ_{523} = -9.54 \text{ kJ mol}^{-1}$$
$$K_{eq_{523}} = 2.174 \times 10^{1}.$$

Gas-phase reactions (3) and (4) may be ruled out on the basis that formaldehyde and formic acid were never detected in the gaseous product mixture. For reaction (2), the observed yield of methyl formate was 3–20 times greater than the equilibrium yield predicted. On the other hand, the yield of methyl formate was always less than or equal to that predicted for reaction

TABLE 5

Comparison of the Theoretical Equilibrium Yields of Methyl Formate for the Reaction CH_3OH + CO = $HCOOH_3$ with Those Found Experimentally at 523 K ($K_p = 5.26 \times 10^{-4}$)

Catalyst	Φ[a]
Cu/ZnO undoped	0.19
0.13 mol% Cs/Cu/ZnO	0.43
0.26 mol% Cs/Cu/ZnO	0.30
0.34 mol% Cs/Cu/ZnO	0.44
0.85 mol% Cs/Cu/ZnO	0.56
1.7 mol% Cs/Cu/ZnO	0.74
2.13 mol% Cs/Cu/ZnO	0.74

[a] Ratio of the observed yield of methyl formate to the calculated equilibrium yield.

(1) under the reaction conditions used, based on the theoretical equilibrium constant and the exit gas composition. This is demonstrated in Table 5 where the ratio Φ of the observed yield of methyl formate to the calculated equilibrium yield is tabulated as a function of cesium loading for the calcined-doped catalysts, and in Fig. 13A where it is shown as a function of reaction temperature for the 0.34 mol% cesium calcined-doped catalyst. Increasing the reaction temperature increased the ratio from 0.2 to 0.9, with the upper limit leveling off at this value. As would be expected at a given temperature, an increase in contact time (decrease in GHSV) increased the yield of methyl formate until the thermodynamic limit was reached. This is shown in Fig. 13B where, at 554 K, an increase in contact time of reactants over the cesium doped Cu/ZnO catalyst showed an asymptotic increase in the ratio Φ toward 1.

Similar temperature effects on the yields of methanol and higher oxygenates over the cesium doped Cu/Zn/Al catalysts were observed as shown in Figs. 8 and 9. An increase in the reaction temperature above 570 K led to a drop in methanol yield predominantly because of thermodynamic limitations; however, the conversion of methanol to higher-molecular-weight products also was a contributing factor. As anticipated, the methyl formate yield was thermodynamically controlled under these conditions, and the value of Φ calculated in the temperature range 560–596 K varied from 0.86 to 1.25. Above 560 K the plot of the logarithmic rate of methyl formate formation vs $1/T$ was linear with a negative slope, as shown in Fig. 9.

Conclusions on the interrelationship between methanol, methyl formate, and ethanol formation rates can be drawn from the analysis of the thermodynamic, isotope, and apparent activation energy data. From the thermodynamic and isotope analysis summarized in Tables 1, 3, and 5 and Figs. 10, 11, and 13, the most likely reaction

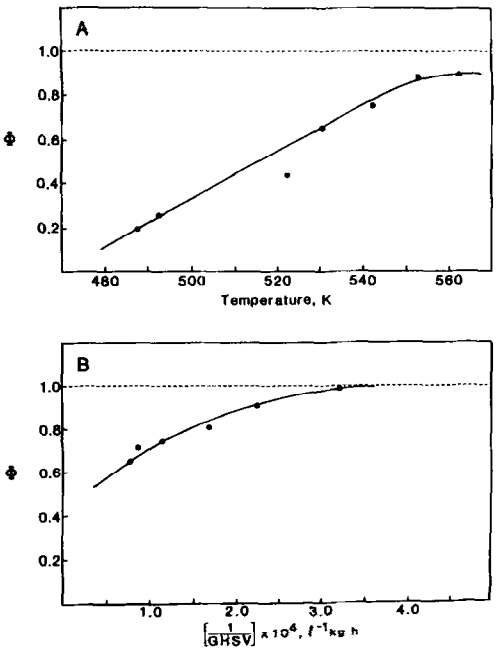

FIG. 13. Effect of temperature (A) with GHSV = 6120 liter(STP)/kg cat./h and of contact time (B) at 554 K on the value of Φ, defined as the ratio of methyl formate yield observed to the predicted thermodynamic yield by reaction (1). Contact time is defined as reciprocal space velocity. Catalyst is 0.34 mol% cesium calcined-doped catalyst and the other experimental conditions are given in Fig. 1. Thermodynamic equilibrium Φ = 1 is marked by a dashed line.

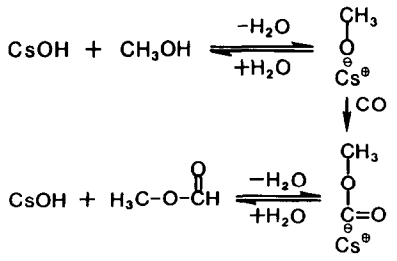

SCHEME II

mechanisms for methyl formate formation involve methanol and CO as primary reactants in a stoichiometry of 1 : 1. Our observed activation energy of 79.6 kJ mol^{-1} for methyl formate can be compared with that found by Tonner *et al.* (*21*) for the homogeneous carbonylation of methanol catalyzed by sodium methoxide (67.7 kJ mol^{-1}). Their reaction was shown to occur through the direct coupling of an intermediate methoxy anion and CO. Over the Cs/Cu/ZnO catalysts, the same mechanism appears to operate, where the methyl group of methyl formate originates from methanol and the carbonyl is derived from CO in the synthesis gas. Scheme II shows the methyl formate-generating mechanism for the Cs dopant on the Cu/ZnO catalyst.

Theoretical investigations of the interaction between CO and a free methoxide ion, Eq. (10), were carried out by Klier *et al.* (*60*) using the MNDO method for electronic energy calculations with the McIver–Komornicki–Powell sigma method for geometry optimization of the transition state as imbedded in the MOPAC/2 Program (*61*). The results showed that no activation barrier exists for reaction (10) and that the nucleophilic attack of CO by the methoxide anion is strongly exothermic,

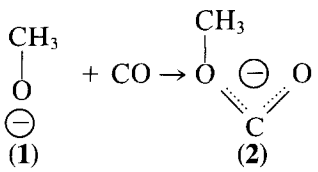

(10)

The rearrangement of the intermediate species by methyl transfer that could lead to carbon–carbon bond formation (11), was found to have a high activation energy (257 kJ mol^{-1}) in spite of the sum of reactions (10) and (11) being exothermic overall,

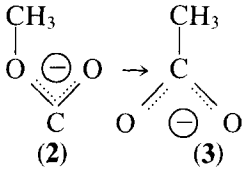

(11)

The energetics along the reaction coordinate for both steps are shown in Fig. 14. The transition state for the rearrangement reaction was identified as having met the criteria described by Murrell and Laidler (*62*). Since the activation barrier for the overall reaction is very high even if the process proceeds adiabatically from **1** to **3** through **2,** the system evidently finds a more favorable hydrolytic pathway as shown in (12), which is the final step in Scheme II. Thus, methyl formate is formed before the acetate ion can be formed by reaction (11),

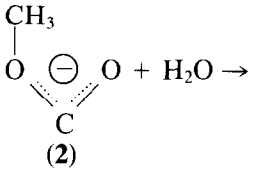

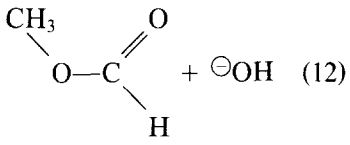

(12)

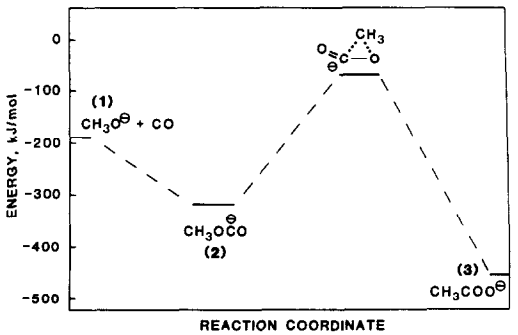

FIG. 14. MNDO energy diagram for the reaction of carbon monoxide with methoxide to form methyl formate.

Since the degree of ^{13}C enrichment of the methyl group of methyl formate was close to that for methanol over the entire temperature range used, methanol in the gas phase must have been in rapid equilibrium with the adsorbed methoxide. In fact, several studies have shown that alcohols such as methanol readily react with the surfaces of basic oxides such as ZnO to give adsorbed methoxides (*53, 63, 64*) even at 300 K (*65*). The most effective adsorption sites in the present case are considered to be the surface cesium cations. The methoxide counterions associated with Cs^+ are more nucleophilic and thus more reactive toward carbonylation than those on the undoped surface. This is supported by the observation that the Φ values in Table 5 increase dramatically in going from the undoped to the 2.13 mol% Cs doped catalyst.

Over the 0.8 mol% cesium doped ternary Cu/Zn/Al catalysts, the yield of methyl formate was again consistent with CO and methanol being the primary reactants as shown in Fig. 9. The yield of methyl formate did not exceed, within experimental error, the predicted thermodynamic yield over a wide temperature range. In addition, from the slope of the plot in Fig. 9 the experimental reaction enthalpy ΔH can be calculated for temperatures above 560 K. The theoretical value of ΔH for reaction (1) is not greatly affected by temperature, changing from -38.04 kJ mol^{-1} at 298 K to -37.8 kJ mol^{-1} at 523 K (*59*). The ΔH value obtained from Fig. 9 is -36.5 kJ mol^{-1}, thus further supporting the reaction route for the formation of methyl formate by Scheme II.

It should be noted that esterification of an adsorbed formate by methanol

$$HCOO^{\ominus} + CH_3OH \rightarrow HCOOCH_3 + {}^{\ominus}OH \quad (13)$$

coupled with a rapid regeneration of the formate

$$CO + {}^{\ominus}OH \rightarrow HCOO^{\ominus} \quad (14)$$

also has the overall stoichiometry of reaction (1) and moreover would result in the observed isotopic composition of methyl formate from labeled methanol and unlabeled CO. This path cannot be excluded by the present data although it is considered less likely than that shown in Scheme II due to steric hindrance in reaction (13).

The "hemiacetal" route to methyl formate from adsorbed methoxide and formaldehyde

$$CH_3O^{\ominus} + H_2CO \rightarrow [CH_3OCH_2O^{\ominus}] \rightarrow HCOOCH_3 + H^{\ominus} \quad (15)$$

that has been suggested to be a mechanistic route over the copper-based catalysts (*5, 23, 24*) is apparently ineffective compared with the CO insertion shown in Scheme II. In the "hemiacetal" route (15), the source of the carbonyl carbon is adsorbed formaldehyde that is expected to be enriched with ^{13}C by equilibration with [^{13}C]methanol. Thus the hemiacetal mechanism would predict the ^{13}C label to be located in both the methyl and the carbonyl group of methyl formate, contrary to the experimental result.

Formation of Ethanol

The high enrichment of ^{13}C in ethanol synthesized from $^{13}CH_3OH$ and $^{12}CO/H_2$ (cf. Table 3) shows that methanol is a major source of both carbons of ethanol. Moreover, the observed isotope composition of singly and doubly ^{13}C-labeled ethanol molecules provides for distinguishing between three classes of mechanisms for ethanol formation, as detailed in Appendix II. The three distinctive mechanistic classes are homologation of methanol via a CO insertion mechanism represented by Eq. (M-1) in Appendix II; homologation of methanol by CO via a symmetric intermediate, such as one suggested by Mazanec (*35*) represented by Eq. (M-2) in Appendix II; and coupling of two methanol molecules represented by Eq. (M-3) in Appendix II. In Table 6, the relative efficiencies $R_{M\text{-}1}$, $R_{M\text{-}2}$, and $R_{M\text{-}3}$ of the three mechanisms, calculated from the NMR data of Table 3 and the GC analyses of Table 4, are given. The

TABLE 6

Fractions of $^{13}CH_3{}^{12}CH_2OH$ (F_x), $^{12}CH_3{}^{13}CH_2OH$ (F_y), and $^{13}CH_3{}^{13}CH_2OH$ (F_z) Observed after Injection of $^{13}CH_3OH$ into $^{12}CO/H_2$, and the Relative Efficiencies[a] R_{M-1}–R_{M-3} of Mechanisms (M-1) to (M-3) over the Cs/Cu/ZnO Catalyst

Temperature (K)	Obs.[b] F_z	Calc.[c] p	Calc.[c] $\frac{F_x^e}{F_z}$	Obs. $\frac{F_x}{F_z}$	Calc.[c] $\frac{F_y^e}{F_z}$	Obs. $\frac{F_y}{F_z}$	R_{M-1}	R_{M-2}	R_{M-3}
522	0.02356	0.1535	5.514	9.34	5.514	8.26	0.06	0.30	0.65
532	0.01031	0.1015	8.850	7.98	8.850	6.44	0.10	−0.31	1.21
543	0.01140	0.1068	8.368	8.68	8.368	7.60	0.06	−0.09	1.03

[a] R_{M-1}, R_{M-2}, and R_{M-3} are quantities derived from the measured F_x, F_y, and F_z. Standard error analysis shows that the absolute standard deviation error in R_{M-1} is ±0.03, in R_{M-2} is ±0.13, and in R_{M-3} is ±0.15 if the relative error in F_x, F_y, and F_z is ±5%.

[b] Determined from observed NMR intensities and GC analyses by using Eq. (A-4) and the procedure outlined in Appendix II.

[c] $p = \sqrt{F_z}$; $F_x^e = F_y^e = p(1 - p)$.

calculation utilizes the observed fractions F_x, F_y, and F_z of the $^{13}CH_3{}^{12}CH_2OH$, $^{12}CH_3{}^{13}CH_2OH$, and $^{13}CH_3{}^{13}CH_2OH$ molecules for the determination of R_{M-1}, R_{M-2}, and R_{M-3} by the procedure outlined in Appendix II.

Although the values of R_{M-1}, R_{M-2}, and R_{M-3} are burdened by a considerable error, especially at low temperatures, it appears that at all temperatures studied the methanol coupling mechanism (M-3) dominates since $R_{M-3} > R_{M-2}, R_{M-1}$. At 543 K where the NMR data are most accurate, the values of R_{M-1}, R_{M-2}, and R_{M-3} support the conclusion that the mechanism (M-3) operates exclusively ($R_{M-3} \approx 1$, $R_{M-1} \approx 0$, $R_{M-2} \approx 0$).[4] This result rules out, over the present catalyst, several earlier proposed C–C bond-forming mechanisms. These include class (M-1) mechanisms via insertion of CO into the C–O bond of methoxide to form acetate that is hydrogenated to ethanol as originally proposed by Fischer (*34*) and later invoked by Natta *et al.* (*1*) and Vedage *et al.* (*5*), CO insertion into a methyl–metal bond proposed as the chain growth step in several mechanistic studies of Fischer–Tropsch synthesis (*30–32*) if the methyl group would originate from methanol, and conversion of methyl formate (formed by reaction Scheme II above) to acetic acid or acetate that is subsequently hydrogenated to ethanol. Also ruled out are class (M-2) mechanisms including CO insertion into adsorbed formaldehyde forming a symmetric glycolate that is subsequently hydrogenated to ethanol as proposed by Mazanec (*35*).

The acceptable mechanisms must fall into class (M-3), and one such previously proposed mechanism involves the nucleophilic attack of an adsorbed formyl on formaldehyde as suggested by Fox *et al.*(*37*). Both the adsorbed formyl and the reacting formaldehyde must be preferentially formed from methanol in order for the Fox *et al.* mechanism to qualify as the present (M-3). The whole reaction sequence due to this modified Fox *et al.* mechanism is represented in Scheme III. Alternative mechanisms that satisfy class (M-3) involve an S_N2 attack on methanol by formyl as represented in Scheme IV or coupling of formyl with an adsorbed CH_x fragment as suggested by Kiennemann *et al.* (*67, 68*) for Rh

[4] The relative efficiencies of mechanisms (M-1)–(M-3) over alkali MoS_2 and alkali CoS–MoS_2 catalysts are diametrically different and the CO insertion mechanism (M-1) dominates over these catalysts ($R_{M-1} \approx 1$, $R_{M-2} \approx 0$, $R_{M-3} \approx 0$) (*66*). Thus the C–C bond-forming reaction steps are uniquely determined by the catalyst used.

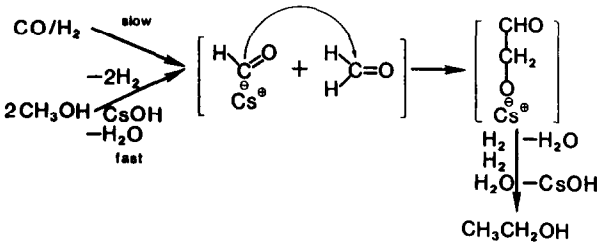

SCHEME III

catalysts. The CH_x fragments can also be hydrogenated to methane (*14, 68*) which, however, is only a trace product over the present Cs/Cu/ZnO catalyst and therefore a mechanism involving the intermediacy of CH_x is unlikely.

Schemes III and IV thus remain the most prominent ones for the $C_1 \rightarrow C_2$ synthetic step over the Cs/Cu/ZnO catalyst (although Scheme IV is considered less likely for steric reasons), and they both involve adsorbed formyl. The chemistry of this species has previously been considered to be important in CO/H_2–amine and methanol–amine coupling reactions (*15, 18, 69*) and its existence has been inferred from trapping reactions with CH_3I to form acetaldehyde (*14*). Spectroscopic evidence has been put forward for the presence of formyl on the surface of the present type of catalysts (*16, 17*).

On the basis of the mechanisms written above, the net charge carried by the formyl species, its orientation, and polarity are of great interest. In organometallic complexes containing formyl, the carbon atom has been shown to have a considerable carbene character (*70, 71*) that results in unexpected lengthening of the C–O bond and lowering of its vibrational frequency and implies a negative charge of this species. Similar low-frequency positions of the C–O group of the reported adsorbed formyls have been observed over ZnO and Cu/ZnO (*16, 54*).

SUMMARY

Cesium doping of the Cu/ZnO catalyst significantly enhances the rates of formation of methanol, methyl formate, and ethanol from CO/H_2. While high methanol selectivity can be maintained at low temperatures and high H_2/CO ratios, the higher oxygenates become more significant products as the temperature increases and the H_2/CO ratio decreases. The C_1 surface species that is readily formed from methanol is a precursor of the methyl group of methyl formate and of both the CH_3 and the CH_2 groups of ethanol. Methyl formate is formed by methanol carbonylation and is not a precursor of ethanol. The C–C bond in ethanol is made by coupling of the C_1 surface intermediates originating from methanol. This mechanism is specific to the present Cs/Cu/ZnO catalyst system, and different CO insertion mechanisms can operate over other types of catalysts, e.g., on alkali MoS_2 catalysts (*66*). For the present Cs/Cu/ZnO and related Cu/ZnO catalysts,

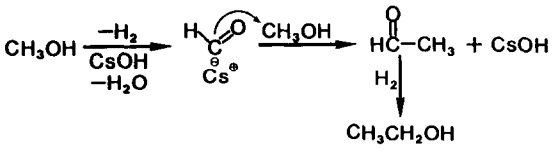

SCHEME IV

evidence based on chemical trapping, ^{13}C label flow, and spectroscopic observations, as well as quantum chemical calculations, supports a mechanism in which adsorbed formyl is a reactive nucleophile that forms the C–C bond by attacking the electropositive carbon of adsorbed formaldehyde or methanol.

APPENDIX I

Accurate carbon and oxygen mass balances of the reactants entering the system and products exiting the system were determined from on-line GC analytical data. The error in the carbon balance was found to be less than 0.5% as shown in column 2 in Table A1 for each reaction temperature indicated in column 1. A ^{13}C balance was also calculated by comparison of the ^{13}C injected into the system as enriched methanol, column 2, to the ^{13}C exiting the reaction and collected as liquid products, column 3. The quantity of ^{13}C unaccounted for, column 4, was expressed as a percentage fraction of the total CO in the effluent stream, column 5. Added to the natural abundance of 1.1% in the CO gas, the total ^{13}C content in exit CO was obtained, column 6. The ^{13}C enrichment of CO was negligible in accounting for the significant enrichment observed in all product molecules. This was especially significant in the high percentage of doubly labeled ethanol evidenced by the doublets arising from coupling of adjacent ^{13}C atoms in the CH_3 and CH_2 groups of ethanol.

APPENDIX II

Fractions of ^{13}C-Labeled Ethanol Molecules

The fractions of the three ^{13}C-labeled ethanol species, $^{13}CH_3{}^{13}CH_2OH$, $^{13}CH_3{}^{12}CH_2OH$, and $^{12}CH_3{}^{13}CH_2OH$, have been calculated from the ^{13}C NMR intensities and the molar concentrations of ethanol (EtOH) and methyl formate (MF) in the product utilizing the carbonyl ^{13}C signal in MF as internal reference. It has been established independently that the carbonyl group of MF has native abundance of ^{13}C, 1.1%, in all the present isotope experiments (*51*). For clarity the NMR signals used are represented in Scheme V.

The satellite doublets around each car-

TABLE A1

A Comparison of Carbon Balances from GC Analyses (Column 2) and Carbon-13 Balance (Columns 3–6) during Injection of Enriched Methanol into the Synthesis Gas as a Function of Temperature

Reaction temperature (K)	% Error in the total carbon balance from GC analyses	^{13}C IN as methanol (mol/kg cat.//h)	^{13}C OUT as liquid product (mol/kg cat./h)	^{13}C balance,[a] (mol/kg cat./h)	^{13}C content[b] of the total exit CO (%)
490	0.018	1.455	1.331	−0.124	1.245
501	0.123	1.455	1.467	+0.012	1.100
513	0.127	1.455	0.959	−0.496	1.660
523	0.172	1.455	1.211	−0.244	1.384
532	0.239	1.455	0.938	−0.517	1.703
543	0.357	1.455	0.925	−0.530	1.729

[a] ^{13}C balance is given by the difference between ^{13}C OUT in column 4 and ^{13}C IN in column 3. The negative numbers indicate unaccounted for ^{13}C. The positive balance is generated by accumulated experimental error.

[b] Calculated from unaccounted for ^{13}C in column 5.

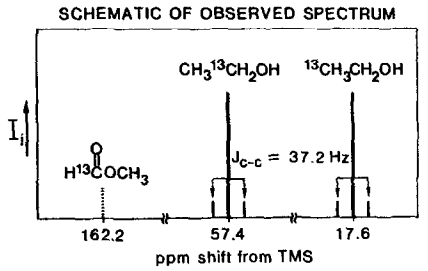

SCHEME V

bon of ethanol marked with $J_{C-C} = 37.2$ Hz are due to exchange coupling between the two carbons of $^{13}CH_3{}^{13}CH_2OH$ and have been used for quantitative determination of the fraction of doubly labeled ethanol molecules. The possibility of the doublets being spinning sidebands has been eliminated by standard procedures that include verifying the independence of the frequency separation of the doublet on the sample spinning rate. The center peaks between the doublets are the resonances of ethanol molecules singly labeled at the carbon marked ^{13}C in Scheme V.

In the analytical calculations, I_i is the intensity of the NMR signal corresponding to species i, i.e.,

I_1, of ^{13}C carbonyl in MF;
I_2, of $^{13}CH_2$ in $^{12}CH_3{}^{13}CH_2OH$;
I_3, of $^{13}CH_2$ in $^{13}CH_3{}^{13}CH_2OH$;
I_4, of $^{13}CH_3$ in $^{13}CH_3{}^{12}CH_2OH$; and
I_5, of $^{13}CH_3$ in $^{13}CH_3{}^{13}CH_2OH$.

Here I_3 and I_5 are given by the sum of the doublet peak heights of $^{13}CH_3$ and $^{13}CH_2$ groups of ethanol, respectively. The total number of ^{13}C gram atoms in a unit volume of the product sample is denoted as

u, the total number of ^{13}C gram atoms per unit volume of the product sample;

N_{MF}, the number of mols of MF per unit volume;

N_E, the number of mols of EtOH per unit volume;

x, the number of mols of $^{13}CH_3{}^{12}CH_2OH$ per unit volume;

y, the number of mols of $^{12}CH_3{}^{13}CH_2OH$ per unit volume; and

z, the number of mols of $^{13}CH_3{}^{13}CH_2OH$ per unit volume.

Then

$$\mathbf{u} = N_{MF} \times 0.011 \sum_{i=1}^{5} I_i/I_1, \quad \text{(A-1)}$$

where the factor 0.011 stands for the natural abundance fraction of ^{13}C in the carbonyl group of MF. The total number of ^{13}C gram atoms in $^{13}CH_3{}^{13}CH_2OH$ per unit volume is equal to $\mathbf{u}(I_3 + I_5)/\Sigma_i I_i$ and the total number z of $^{13}CH_3{}^{13}CH_2OH$ moles per unit volume is equal to one-half that number,

$$z = \frac{1}{2}\,\mathbf{u}\,\frac{(I_3 + I_5)}{\sum_i I_i}. \quad \text{(A-2)}$$

Combination of (A-1) and (A-2) gives

$$z = \frac{1}{2} = N_{MF} \times 0.011\,\frac{(I_3 + I_5)}{I_1}. \quad \text{(A-3)}$$

Hence the fraction F_z of $^{13}CH_3{}^{13}CH_2OH$ among all ethanol isotope species is

$$F_z = \frac{z}{N_E} = \frac{1}{2}\,\frac{N_{MF}}{N_E}\,\frac{(I_3 + I_5)}{I_1} \times 0.011. \quad \text{(A-4)}$$

Similarly the fractions $F_x = (x/N_E)$ and $F_y = (y/N_E)$ of $^{13}CH_3{}^{12}CH_2OH$ determined from the NMR and GC analyses are

$$F_x = \frac{N_{MF}}{N_E}\,\frac{I_4}{I_1} \times 0.011 \quad \text{and}$$

$$F_y = \frac{N_{MF}}{N_E}\,\frac{I_2}{I_1} \times 0.011. \quad \text{(A-5)}$$

Denote further $F_z = p^2$ where p is the probability of finding two ^{13}C atoms simultaneously in an equilibrium mixture of $^{13}CH_3{}^{13}CH_2OH$, $^{13}CH_3{}^{12}CH_2OH$, $^{12}CH_3{}^{12}CH_2OH$. The so-defined p provides for the determination of whether the observed mixture of isotopically labeled ethanol molecules actually is or is not in statistical equilibrium, and this in turn is used to distinguish between the principal classes of mechanisms

for ethanol formation,

$$^{13}CH_3OH + {}^{12}CO/H_2 \rightarrow {}^{13}CH_3{}^{12}CH_2OH \quad \text{(M-1)}$$

$$^{13}CH_3OH + {}^{12}CO/H_2 \rightarrow \tfrac{1}{2}[{}^{13}CH_3{}^{12}CH_2OH + {}^{12}CH_3{}^{13}CH_2OH] \quad \text{(M-2)}$$

$$2\,{}^{13}CH_3OH \rightarrow 2[F_x^e({}^{13}CH_3{}^{12}CH_2OH) + F_y^e({}^{12}CH_3{}^{13}CH_2OH) + F_z^e({}^{13}CH_3{}^{13}CH_2OH)] \quad \text{(M-3)}$$

Mechanisms (M-1) and (M-2) do not give rise to doubly labeled ethanol molecules (except those with native ^{13}C concentration which are neglected) and only mechanism (M-3) gives rise to the statistical distribution of ^{13}C among the three ^{13}C-labeled molecular species.

If mechanism (M-3) operates simultaneously with (M-1) and (M-2), no statistic equilibrium can be reached. Further, mechanism (M-2) can be distinguished from (M-1) in that (M-2) results in equal concentrations of ^{13}C in the two singly labeled species $^{13}CH_3{}^{12}CH_2OH$ and $^{12}CH_3{}^{13}CH_2OH$ whereas (M-1) produces only $^{13}CH_3{}^{12}CH_2OH$. The Fox *et al.* mechanism (*37*) falls into the (M-3) category, the Mazanec mechanism (*35*) corresponds to the (M-2) category, and a CO insertion mechanism into a methyl–metal bond or into the C–O bond of methoxide (*30–32*) falls into the (M-1) category.

From $p = \sqrt{F_z}$, the fractions F_x^e of $^{13}CH_3{}^{12}CH_2OH$ and F_y^e of $^{12}CH_3{}^{13}CH_2OH$ that would be in isotopic equilibrium with the doubly labeled ethanol are

$$F_x^e = F_y^e = p(1 - p). \quad \text{(A-6)}$$

These are the fractions theoretically predicted from the observed fraction F_z of the doubly labeled ethanol if the mechanism (M-3) operates exclusively. Any difference between the observed F_x and F_x^e or F_y^e must then be attributed to mechanisms (M-1) and (M-2), the extent of which can be further determined using the difference between F_x and F_y.

We now define the relative efficiencies of mechanisms (M-1) to (M-3) as $R_{M\text{-}1}$ to $R_{M\text{-}3}$ as

$$R_{M\text{-}1} = (F_x - F_y)/\theta;$$
$$R_{M\text{-}2} = 2(F_y - F_y^e)/\theta;$$
$$R_{M\text{-}3} = (F_x^e + F_y^e + F_z)/\theta, \quad \text{(A-7)}$$

where $\theta = (F_x + F_y + F_z)$. That these indices are relative efficiencies of the three mechanisms follows from the properties that $R_{M\text{-}3} = 0$ when $F_z = 0$ and $R_{M\text{-}3} = 1$ when $F_x = F_x^e$, $F_y = F_y^e$, and $F_z \neq 0$, i.e., when the $^{13}CH_3{}^{12}CH_2OH$, $^{12}CH_3{}^{13}CH_2OH$, and $^{13}CH_3{}^{13}CH_2OH$ molecules are in statistical equilibrium as dictated by mechanism (M-3); $R_{M\text{-}2} = 0$ when $F_y = F_y^e$ and $R_{M\text{-}2} = 1$ when $F_z = 0$ and $F_x = F_y$ as dictated when (M-2) operates exclusively; and $R_{M\text{-}1} = 0$ when $F_x = F_y$ and $R_{M\text{-}1} = 1$ when $F_y = F_z = 0$ as dictated when (M-1) alone operates. The values of $R_{M\text{-}1}$, $R_{M\text{-}2}$, and $R_{M\text{-}3}$ are given in Table 6 for the present catalyst.

ACKNOWLEDGMENTS

This work was supported in part by U.S. Department of Energy Contracts DE-FG22-83PC60786 and DE-AC22-84PC70021. We appreciate the technical assistance of Donna Mitko and Roy Bastian. C.E.B. is pleased to acknowledge the receipt of Buch, Horner, and Texaco Fellowships via Lehigh University.

REFERENCES

1. Natta, G., Colombo, U., and Pasquon, I., *in* "Catalysis" (P. H. Emmett, Ed.), Vol. V, Chap. 3. Reinhold, New York, 1957.
2. Smith, K. J., and Anderson, R. B., *Canad. J. Chem. Eng.* **61,** 40 (1983).
3. Klier, K., *in* "Catalysis on the Energy Scene" (S. Kaliaguine and A. Mahay, Eds.), p. 439. Elsevier, Amsterdam, 1984.
4. Morgan, G. T., *Proc. R. Soc. London A* **127,** 246 (1930); Morgan, G. T., Hardy, D. V. N., and Procter, R. H., *J. Soc. Chem. Ind.* **51,** 1T (1932).
5. Vedage, G. A., Himelfarb, P. B., Simmons, G. W., and Klier, K., *ACS Symp. Ser.* **279,** 295 (1985).
6. Hofstadt, C. E., Kochloefl, K., and Bock, O., German Patent 3,005,551 (Aug. 20, 1981), assigned to Süd-Chemie AG.
7. Kihuzono, Y., Kagami, S., Naito, S., Onishi, T., and Tamaru, K., *J. Chem. Soc. Faraday Discuss.* **72,** 135 (1982).
8. Davies, P., and Snowdon, F. R., U.S. Patent

3,326,956 (June 20, 1967); Collins B. M., U.S. Patent 3,850,850 (Nov. 26, 1974), assigned to Imperial Chemical Industries Ltd.; Stiles, A. B., U.S. Patent 4,111,847 (Sept. 5, 1978), assigned to E. I. DuPont de Nemours and Co.

9. Nunan, J., Klier, K., Young, C. W., Himelfarb, P. B., and Herman, R. G., *J. Chem. Soc. Chem. Commun.*, 193 (1986).
10. Klier, K., Herman, R. G., Nunan, J. G., Smith, K. J., Bogdan, C. E., Young, C.-W., and Santiesteban, J. G., *in* "Methane Conversion" (D. M. Bibby, C. D. Chang, R. F. Howe, and S. Yurchak, Eds.), p. 109. Elsevier, Amsterdam, 1988.
11. Kung, H. H., *Catal. Rev. Sci. Eng.* **22,** 235 (1980); Klier, K., "Advances in Catalysis" (D. D. Eley, P. W. Selwood, and P. B. Weisz, Eds.), Vol. 31, p. 243. Academic Press, San Diego, 1982.
12. Edwards, J. F., and Schrader, G. L., *J. Phys. Chem.* **88,** 5620 (1984); *J. Catal.* **94,** 175 (1985).
13. Deluzarche, A., Kieffer, R., and Muth, A., *Tetrahedron Lett.* **38,** 3357 (1977).
14. Deluzarche, A., Hindermann, J. P., Kiennemann, A., and Kieffer, R., *J. Mol. Catal.* **31,** 225 (1985).
15. Vedage, G. A., Pitchai, R., Herman, R. G., and Klier, K., "Proceedings, 8th International Congress on Catalysis, Berlin, 1984," Vol. II, p. 47. Dechema, Frankfurt-am-Main, 1984.
16. Saussey, J., Lavalley, J. C., Lamotte, J., and Rais, T., *J. Chem. Soc. Chem. Commun.*, 278 (1982).
17. Lavalley, J. C., Saussey, J., and Rais, T., *J. Mol. Catal.* **17,** 289 (1982).
18. Vedage, G. A., Herman, R. G., and Klier, K., *J. Catal.* **95,** 423 (1985).
19. Gjaldbaek, J. C., *Acta Chim. Scand.* **2,** 683 (1948).
20. Aguilo, A., and Horlenko, T., *Hydrocarbon Proc.* **59**(11), 120 (1980).
21. Tonner, S. P., Trimm, D. L., and Wainwright, M. S., *J. Mol. Catal.* **18,** 215 (1983).
22. Cant, N. W., Tonner, S. P., Trimm, D. L., and Wainwright, M. S., *J. Catal.* **91,** 197 (1985).
23. Takahashi, K., Takezawa, N., and Kobayashi, H., *Chem. Lett.* **7,** 1061 (1983).
24. Denise, B., and Sneeden, R. P. A., *C_1 Mol. Chem.* **1,** 307 (1985).
25. Mueller, L. L., and Griffin, G. L., *J. Catal.* **105,** 352 (1987).
26. Sorum, P. A., and Onsager, O. T., "Proceedings, 8th International Congress on Catalysis, Berlin, 1984," Vol. II, p. 233. Dechema, Frankfurt-am-Main, 1984.
27. Smith, K. J., Young, C.-W., Herman, R. G., and Klier, K., submitted for publication.
28. Takeuchi, A., and Katzer, J. R., *J. Phys. Chem.* **86,** 2438 (1982); Takeuchi, A., Katzer, J. R., and Crecely, R. W., *J. Catal.* **82,** 474 (1983).
29. Kagami, S., Naito, S., Kikuzono, Y., and Tamaru, K., *J. Chem. Soc. Chem. Commun.*, 256 (1983).
30. Wender, I., Friedman, S., Steiner, W. A., and Anderson, R. B., *Chem. Ind.*, 1694 (1958).
31. Pichler, H., and Schulz, H., *Chem. Ing. Tech.* **42,** 1162 (1970).
32. Henrici-Olivé, G., and Olivé, S., *Angew. Chem. Int. Ed.* **15,** 136 (1976).
33. Sachtler, W. M. H., "Proceedings, 8th International Congress on Catalysis, Berlin, 1984," Vol. I, p. 151. Dechema, Frankfurt-am-Main, 1984.
34. Fischer, F., *Ind. Eng. Chem.* **17,** 576 (1925); "Conversion of Coal into Oils," p. 251. Van Nostrand, New York, 1925.
35. Mazanec, T. J., *J. Catal.* **98,** 115 (1986).
36. Graves, G. D., *Ind. Eng. Chem.* **23,** 1381 (1931).
37. Fox, J. R., Pesa, F. A., and Curatolo, B. S., *J. Catal.* **90,** 127 (1984).
38. Himelfarb, P. B., Simmons, G. W., Klier, K., and Herman, R. G., *J. Catal.* **93,** 442 (1985).
39. Herman, R. G., Klier, K., Simmons, G. W., Finn, B. P., Bulko, J. B., and Kobylinski, T. P., *J. Catal.* **56,** 407 (1979).
40. Himelfarb, P. B., Ph.D. dissertation, Department of Materials Science and Engineering, Lehigh University, 1986; Himelfarb, P. B., Simmons, G. W., Nunan, J. G., and Klier, K., "193rd National Meeting of the American Chemical Society, Denver, CO," Abstr. No. COLL-124, April 1987.
41. Herman, R. G., Simmons, G. W., and Klier, K., "Proceedings, 7th International Congress on Catalysis, Tokyo, 1980" (T. Seiyama and K. Tanabe, Eds.), p. 475. Elsevier, Amsterdam, 1981.
42. Ruggeri, O., Tredici, A., Trifiro, F., and Vaccari, A., "8th Pan-Am. Symp. Catal., Huelva, Spain, 1982"; Trifiro, F., Vaccari, A., Del Piero, G., Fattore, V., and Notari, B., *in* "Proc. 5th Intern. Symp. Heterogeneous Catal." (D. Shopov, A. Andreev, A. Palazov, and L. Petrov, Eds.), Vol. II, p. 303. Bulgarian Acad. Sci., Sofia, 1983.
43. Courty, P., and Marcilly, C., *in* "Preparation of Catalysts III" (G. Poncelet, P. Grange, and P. A. Jacobs, Eds.), p. 485. Elsevier, Amsterdam, 1983.
44. Busetto, C., Del Piero, G., Manara, G., Trifiro, F., and Vaccari, A., *J. Catal.* **85,** 260 (1984).
45. Bulko, J. B., Herman, R. G., Klier, K., and Simmons, G. W., *J. Phys. Chem.* **83,** 3118 (1979).
46. Herman, R. G., *in* "Catalytic Conversions of Synthesis Gas and Alcohols to Chemicals" (R. G. Herman, Ed.), p. 433. Plenum, New York, 1984.
47. Herman, R. G., Pendleton, P., and Bulko, J. B., *in* "Advances in Materials Characterization" (D. R. Rossington, R. A. Condrate, and R. L. Snyder, Eds.), p. 109. Plenum, New York, 1983.
48. Young, C. W., M.S. thesis, Department of Chemical Engineering, Lehigh University, 1985.
49. Bybell, D. G., Deutsch, P. P., Herman, R. G., Himelfarb, P. B., Nunan, J. G., Young, C. W., Bogdan, C. E., Simmons, G. W., and Klier, K., *Prepr. Div. Pet. Chem. ACS* **31**(1), 282 (1986).
50. Nunan, J. G., Bogdan, C. E., Klier, K., Smith, K.

J., Young, C. W., and Herman, R. G., submitted for publication.
51. Bogdan, C. E., *et al.*, in press.
52. Jackson, N. B., and Ekerdt, J. G., *J. Catal.* **101,** 90 (1986).
53. Bowker, M., Houghton, H., and Waugh, K. C., *J. Chem. Soc. Faraday Trans. 1* **77,** 3023 (1981).
54. Saussey, J., Lavalley, J. C., and Rais, T., *J. Mol. Catal.* **26,** 159 (1984).
55. Chan, L., and Griffin, G. L., *Surf. Sci.* **173,** 160 (1986).
56. Dombek, B. D., Final Technical Report DE-AC22-84PC70022 from Union Carbide Corp. to the U.S. Department of Energy, Jan. 30, 1987.
57. Klier, K., Chatikavanij, V., Herman, R. G., and Simmons, G. W., *J. Catal.* **74,** 343 (1982).
58. Klier, K., Herman, R. G., and Young, C. W., *Prepr. Div. Fuel Chem. ACS* **29**(5), 273 (1984).
59. Reid, R. C., Prausnitz, J. M., and Sherwood, T. K., "The Properties of Gases and Liquids," 3rd ed., McGraw-Hill, New York, 1977.
60. Klier, K., Zeroka, D., and Bybell, D., "189th National Meeting of the American Chemical Society, Miami Beach, FL," Abstract No. COLL-0033, Apr. 1985.
61. Quantum Chemistry Program Exchange, Program No. 455, Chemistry Department, Indiana University, Bloomington, IN.
62. Murrell, J. N., and Laidler, K. J., *Trans. Faraday Soc.* **64,** 371 (1968).
63. Foyt, D. C., and White, J. M., *J. Catal.* **49,** 260 (1977).
64. Ueno, A., Onishi, T., and Tamaru, K., *J. Chem. Soc. Faraday Trans. 1* **67,**3585 (1971).
65. Roberts, D. L., and Griffin, G. L., *J. Catal.* **95,** 617 (1985).
66. Santiesteban, J. G., Bogdan, C. E., Herman, R. G., and Klier, K., "Proceedings, 9th International Congress on Catalysis" (M. J. Phillips and M. Ternan, Eds.), Chem. Inst. Canada, 1988, Vol. 2, pp. 561–568.
67. Breault, R., Hindermann, J. P., Kiennemann, A., and Laurin, M., *Stud. Surf. Sci. Catal.* **19,** 489 (1984).
68. Kiennemann, A., Hindermann, J. P., Breault, R., and Idriss, H., *Prepr. Div. Pet. Chem. ACS* **31**(1), 46 (1986).
69. Klier, K., Herman, R. G., and Vedage, G. A., U.S. Patent 4,642,381 (Feb. 10, 1987), assigned to Lehigh University.
70. Fagan, P. J., Moloy, K. G., and Marks, T., *J. Amer. Chem. Soc.* **103,** 6959 (1981).
71. Marks, T. J., *Science* **217,** 989 (1982).